

**ORIGIN OF THE PRE-TROPICAL STORM DEBBY (2006)
AFRICAN EASTERLY WAVE-MESOSCALE CONVECTIVE SYSTEM**

Yuh-Lang Lin^{1,2,*}, Liping Liu³, Guoqing Tang³, James Spinks², and Wilson Jones³
 Department of Physics¹
 Department of Energy and Environmental Systems²
 Department of Mathematics³
 North Carolina A&T State University, Greensboro, North Carolina

1. INTRODUCTION

It is well documented that most tropical cyclones (TCs) in the main development region (MDR, including tropical North Atlantic and Caribbean Sea, primarily between 10° and 20°N) of Atlantic hurricanes formed from African Easterly Waves (AEWs) (e.g., Carlson 1969; Frank 1970; Goldenberg and Shapiro 1996). Some of the AEWs which did not spawn hurricanes in MDR continued to propagate westward across the Atlantic and then spawned hurricanes in eastern Pacific on the lee of Central American Mountains (e.g., Bister and Emanuel 1997; Farfan and Zehnder 1997). AEW-induced tropical cyclones account for about 60% of the Atlantic basin tropical storms and nonmajor hurricanes, but about 85% of the major hurricanes (categories 3, 4 and 5) (Landsea 1993). Note that the major hurricanes account for just over 20% of the tropical storms and hurricanes that strike the United States but cause more than 80% of the damage (Pielke and Landsea 1998). Thus, understanding the origins and formation mechanisms of the AEWs is essential in improving the forecast of Atlantic hurricanes.

Based on the definition in the Glossary of Meteorology (Glickman 2000), an easterly wave is a migratory wavelike disturbance of the tropical easterlies. It is a wave within the broad easterly current and moves from east to west, generally more slowly than the current in which it is embedded. Thus, African easterly waves may be defined as easterly waves observed over North Africa. In addition, observational analyses indicated that AEWs possess the following basic characteristics (e.g., Chen 2006): (1) propagation speeds of 7 – 9 ms⁻¹, (2) wavelengths of ~2000 – 4000 km, (3) propagating along the rainy zone and to the south of the African easterly jet (AEJ) around 10°N (AEW_s) or along the Saharan thermal low near 20°N (AEW_n) (e.g., Reed et al. 1977; Burpee 1974; Chen 2006), and (4) the maximum intensity of AEWs is near the 700 hPa level. Note that it was also proposed that the vorticity centers of AEW_n and AEW_s propagate together as part of a single AEW (see e.g. Carlson 1969, Burpee 1974, Reed et al. 1977, Pytharoulis and Thorncroft 1995). Similar to the pre-Alberto (2000) AEW (Lin et al., 2005), the pre-Debbly (2006) AEW propagated along 10°N and thus can be identified as a

AEW_s. Several mechanisms have been proposed in the past to explain the formation of AEWs (see Chen 2006 for a brief review). Firstly, the Charney-Stern (1962) barotropic-baroclinic instability was proposed by Burpee (1972), which is more applicable for AEW_ss (e.g., Rennick 1976; Mass 1979; Kwon 1989; Thorncroft and Hoskins 1994a, b). Secondly, the baroclinic instability was proposed by Chang (1993) and Thorncroft (1995), which seems to be more applicable for AEW_ns. This mechanism may include the so-called AEJ instability (e.g., Simmons 1977; Thorncroft and Hoskins 1994a, b; Grist et al. 2002) since the AEJ is supported by the baroclinicity associated with the Sahara desert. Thirdly, the convective heating associated with the intertropical convective zone (ITCZ) has also been proposed to explain the formation of AEWs (e.g., Hsieh and Cook 2005, 2007; Thorncroft et al. 2008). Latent heating may also act together with barotropic/baroclinic instability. Fourthly, the orographic forcing has also been proposed as a formation mechanism of AEWs (Carlson 1969; Mozer and Zehnder 1996; Hill and Lin 2003; Lin et al. 2005; Berry and Thorncroft 2005). In addition, AEWs can also be strengthened by cyclonic vorticity (mesoscale convective vortices – MCVs) produced by MCSs.

These existing mechanisms may help us identify the potential origins of the AEW. However, searching for the origins of AEWs, such as the pre-Debbly AEW, will add new understanding or mechanisms to the list. For example, in searching for the origin of pre-Alberto (2000) AEW and MCS, it was found that orographic forcing associated with EH may serve as a formation mechanism of AEW.

Although a number of previous studies indicated that AEW could not be detected in Eastern Africa (e.g. Burpee 1972), Hill and Lin (2003) and Lin et al. (2005) have traced the pre-Alberto (2000) MCS system and its precursor to the EH and proposed that the AEW-MCS system was initiated by the EH. Analysis of Meteosat satellite imagery indicated about 68% of the eastern Atlantic tropical cyclones originated from the EH region during the period of 1990-2001 (Lin et al. 2005). On the other hand, Berry and Thorncroft (2005) proposed that the pre-Alberto AEW was initiated by convection over the Darfur Mountains. Note that the MCS is not necessarily associated with AEW during their early formation stage in eastern Africa.

AEWs often have MCSs embedded within them while traveling westward (e.g., Payne and McGarry 1977; Laing and Fritsch 1993; Fink and Reiner 2003). These MCSs help modulate rainfall over the African continent on a daily basis (e.g., Carlson 1969) and help

* *Corresponding author address:* Dr. Yuh-Lang Lin, Dept. of Physics, North Carolina A&T State Univ., 1601 E. Market St., Greensboro, NC 27411.
 E-mail: ylin@ncat.edu

make AEWs detectable from the satellite imagery. Based on the analysis of satellite imagery and ECMWF reanalysis data, Mekonnen et al. (2006) found that the Darfur Mountains are particularly important for providing convective precursors that propagate westward and trigger AEWs downstream. On the other hand, as mentioned above, Lin et al. (2005) found that the diurnally-induced MCS over the EH was able to combine with the AEW, which was produced nearby, to form the pre-Alberto AEW-MCS system. In West Africa, some MCSs, such as squall lines and cloud clusters, are found to be modulated by AEWs (Laing et al. 2008).

In this study, we make distinction between the pre-Debby MCS/cloud clusters and AEW, and examine closely the evolution of the pre-Debby (2006) AEW and MCSs in EH, Darfur Mountains (DF), Asir Mountains (AS), and southern Arabian Peninsula to gain more understanding of the origins of the pre-TC AEWs. We also investigate the sources of both the convective cloud clusters and vorticity perturbations and how they were strengthened.

The paper is organized as follows. Section 2 discusses the origin and propagation of the pre-Debby (2006) MCS/cloud clusters, based on the satellite imagery. Section 3 describes the Advanced Research Weather Research and Forecasting (ARW) model and the numerical experiments designed for this study. Section 4 applies the ARW to investigate the origins and propagation of the pre-Debby MCS and AEW. Origins of both the convective cloud clusters and vorticity perturbations prior to the pre-Debby MCS and AEW, respectively, will also be discussed in Section 4. Concluding remarks can be found in Section 5.

2. ORIGIN OF THE PRE-DEBBY (2006) MCS/CLOUD CLUSTERS AND AEW

The Meteosat 8 infrared (IR) images with 6h interval are used to trace the pre-Debby (2006) MCS or cloud clusters (AMMA 2006). The pre-Debby MCS can be traced back to 1800 UTC 16 August (8/16/18Z) 2006 approximately located at (20°E, 12°N) on the lee side of the southwest Darfur Mountains near southeast Chad (denoted as solid yellow circles in Fig. 1b) from its tropical storm stage over the eastern North Atlantic Ocean at 8/22/18Z (Fig. 1d). Before 8/16/18Z, the pre-Debby MCS can be further traced back to EH and AS as a series of cloud clusters (Figs. 1a-1b). For convenience, the general geography of Africa and Arabian Peninsula is provided in Fig. 2a.

2.1 Merging of Cloud Clusters into the Pre-Debby MCS before 1800 UTC August 16

Before 8/16/18Z (Figs. 1a-1b), at first glance, the convective activity prior to the pre-Debby MCS did not seem to occur as a single MCS from the satellite imagery, but rather as a series of successive, more or less organized cloud clusters. During the period 8/8/06Z to 8/10/00Z (not shown), a series of cloud clusters developed at (35-40°E, 10-15°N) over the EH and AS (see Table 1 for abbreviations and Fig. 2 for

geography). These convective clusters went through growing, splitting, advection, weakening, and merging processes, then propagated westward across the North African continent at later times. During these processes, not every individual cloud cluster survived. In fact, some of them propagated faster than the average speed and dissipated while a new MCS or cloud cluster formed. Another series of convective cloud clusters developed on 10-11 August over southwest Arabian Peninsula, Asir Mountains (AS), and EH at (35-45°E, 10-15°N). In fact, three convective cloud clusters over this area at 8/11/00Z can be identified (yellow dotted circle in the upper-right panel of Fig. 1a). In the next 24h, the cloud cluster over EH grew stronger, while the other two cloud clusters over Red Sea and AS dissipated. The cloud cluster over EH then split into two cloud clusters around 8/11/18Z. The cloud cluster on the left started to propagate away from the EH, went through growing and splitting processes while it propagated further downstream prior to the pre-Debby MCS. This cloud cluster is denoted as white dotted circles on the left panels of Fig. 1a.

The upstream (right) cloud cluster at 8/12/00Z over the Red Sea dissipated in the next 12h (dotted yellow circles in Fig. 1a) as it went through the nocturnal cycle of the orographic convection over EH and Red Sea. At 8/12/18Z, this cloud cluster redeveloped over EH and AS mountains. The convective clouds contained in this cloud cluster merged into a single, small, but much stronger cloud cluster around 8/13/06Z. Similar splitting and weakening processes repeated during the period 8/13/06Z to 8/14/00Z (Figs. 1a and 1b). The merged cloud cluster propagated to the northwest of EH by 8/14/00Z (the dotted yellow circle in the upper right panel of Fig. 1b), mainly being advected by the northeasterly mean wind. This cloud cluster developed further in the next 6h, but then broke up into several cloud clusters and covered a larger area by 8/15/06Z. Note that diurnal convection is also frequently observed over the highlands of central and western Africa, such as Air in West Niger, and Jos Plateau in North Nigeria, which tends to enhance the convective cloud clusters.

Based on the satellite imagery, the cloud-merging and splitting processes were quite common for propagating cloud clusters. The cloud-splitting process may be explained by the new cloud clusters developed at the front edges (i.e. gust fronts) of the evaporative-cooling generated outward (westward or eastward) propagating density currents (e.g., Lin 2007). The left (westward) propagating density current, thus the left cloud cluster, propagated westward faster due to addition of the easterly basic wind to the density current propagation. During the downstream (westward) propagation, a cloud cluster went through growing and weakening periods, similar to the genesis and lysis, respectively, periods discussed in Lin et al. (2005). In addition, the generation of new convective cells west of a pre-existing cloud cluster was favored by strong and dry easterly winds in the AEJ at ~ 600-700 hPa. At 8/16/00Z, the cloud cluster over the DF at 8/15/12Z (the dotted yellow circle in the left-upper panel of Fig. 1b) split into two cloud clusters. The upstream (right) cloud

cluster dissipated during the period 8/16/00Z to 8/16/12Z thus became less identifiable, while the downstream (left) cloud cluster disappeared at 8/16/12Z. The upstream cloud cluster, as described above, appears to go through the nocturnal cycle of the diurnal convection over the DF, which grew stronger in the afternoon around 1400 local time (8/16Z/18Z), as can be clearly identified near (20°E, 10°N) (the solid yellow circle in the left-lower panel of Fig. 1b) and afterwards.

Due to its MCS characteristics, i.e. a complex of thunderstorms that becomes organized on a scale larger than the individual thunderstorms and persists for several hours (Houze 1993), and served as a precursor of Tropical Storm Debby (2006), this more-coherent cloud cluster formed after 8/16/18Z may be called “pre-Debby MCS”.

2.2 Evolution of the Pre-Debby MCS after 1800 UTC August 16

The above mentioned pre-Debby MCS grew stronger from 8/16/18Z to around 8/17/06Z (Figs. 1b and 1c), went through splitting process in the next 12h or so (Fig. 1c), and then continued to grow after 8/17/18Z until encountered the Guinea (Futa Jallon) Highlands (GH) around 8/19/12Z (Figs. 1c and 1d). Note that the propagating AEW and MCS or cloud clusters may be weakened or split by orographic blocking, but may be strengthened or weakened by the diurnal heating or cooling over the mountains. This may help explain the discontinuity of the pre-Debby MCS/convective cloud clusters. The relative strength of these forcing depends on several factors, which may be approximately represented by the orographic Froude number (U/Nh , where U is the mean wind speed, N the buoyancy frequency and h the mountain height) and the thermal Froude number (U/Nd , where d is the heating or cooling height; see Lin 2007, p.195). Due to the scope of the problem, it deserves a separate study.

The propagation of this pre-Debby MCS from 8/16/18Z to the Atlantic Ocean was smooth except when it approached GH. During its passage over GH, it appears that convection developed quicker on the lee and southern sides of the mountains during the period 8/20/00Z to 8/20/06Z. At 8/20/06Z, the pre-Debby MCS split into two cloud clusters. The downstream cloud cluster (dotted white circle in the 8/20/06Z panel of Fig. 1d) continued to propagate westward, while the upstream cloud cluster regrouped and developed into a stronger MCS (yellow circle in the left panels of Fig. 1d except 8/20/00Z). This MCS then triggered the Tropical Storm Debby over the ocean after 8/21/00Z. This splitting process over the GH is clearly depicted in the Hovmoller diagram of the brightness temperature analyzed from the grid satellite data (GRISAT) as shown in Fig. 3. The propagation speed of the pre-Debby MCS during the period 8/16/18Z to 8/21/18Z was approximately 7.4 ms^{-1} , slightly faster than the lower end of the climatological mean speed of $7 - 9 \text{ ms}^{-1}$ (Reed et al. 1977) but comparable to that of pre-Alberto (2000) MCS (Lin et al. 2005).

In summary, the pre-Debby MCS can be traced clearly to 8/16/18Z. The pre-Debby MCS was formed by a series of successive, more or less organized cloud clusters during the period 8/11/00Z to 8/16/18Z, which started over the area of EH, AS, and southwest Arabian Peninsula. The nocturnal cycle of the diurnal convection over the mountains tend to suppress the convective activity of these cloud clusters. In the following, we will adopt a mesoscale numerical model to help trace the pre-Debby MCS and the cloud cluster prior to it. In addition, we will also use the Global Forecast System (GFS) analysis data and the ARW mesoscale model to trace the origin of the pre-Debby AEW and its coupling with pre-Debby MCS/cloud clusters.

2.3 Upstream Environments of the Pre-Debby Cloud Clusters and AEW

Due to the lack of observational data over eastern Africa, the upstream environments for the pre-Debby cloud clusters and AEW are examined by using the GFS analysis data. Using the cloud water content of the GFS data, the cloud clusters prior to the pre-Debby MCS can be traced back to EH-AS region in eastern Africa and Arabian Peninsula (Fig. 4). Three to four convective systems or cloud clusters co-existed along the belt of 5-15°N, which are associated with the ITCZ. The ITCZ during the month of August 2006 extended eastward from the eastern Africa near EH-AS region to the southern coast of Arabian Peninsula and Arabian Sea (Fig. 5). In Fig. 4, it can be seen that there were convective clouds over Arabian Sea, but not much convective cloud activities shown over the southern coast of Arabian Peninsula. This seems consistent with the cut-off of cloud water contents east of EH-AS region in the Hovmoller diagram (Fig. 12a).

Figure 6 shows the Hovmoller diagram of the 5-15°N averaged cloud water contents from the WRF simulation data. The pre-Debby MCS/cloud cluster can be approximately traced back to about 42°E, just over AS and the eastern edge of EH. In addition, the pre-Debby MCS analyzed by the GFS (Fig. 4) and simulated by WRF (Fig. 6) moved faster than that analyzed in the satellite imagery and GRISAT data (Figs. 1 and 3).

Based on the GRISAT data (Fig. 3), GFS data (Fig. 4) and WRF simulation (Fig. 6), and NOAA Climate Prediction Center (CPC) Famine Early Warning System (FEWS) net rainfall estimate (Fig. 5), it appears that the cloud clusters prior to the pre-Debby MCS were originated over EH-AS region and downstream (west) of it. In order to trace the origins of the pre-Debby (2006) MCS/cloud clusters, as well as the pre-Debby AEW, we will perform regional modeling simulations using ARW.

3. THE NUMERICAL MODEL AND EXPERIMENTAL DESIGN

The model used for this study is the ARW model version 3.1 (Skamarock et al. 2008). ARW model is a fully compressible, three-dimensional, nonhydrostatic model using terrain-following vertical coordinates. The governing equations for ARW are written in flux-form

with conserved mass and dry entropy. In this study, the Runge-Kutta third-order time scheme is employed, and the fifth- and third-order advection schemes are used for the horizontal and vertical directions, respectively.

For the experiments, we utilize a double-nested, two-way interaction domain as illustrated in Fig. 2. For the outer domain, 24 km horizontal resolution with 384 x 174 horizontal grid intervals is used. In the vertical direction, the grids are stretched from the surface to the model top (20 km) with a total of 28 levels. A 5-km deep sponge layer was added to the upper part of the physical domain. A nudging-relaxation lateral boundary condition is applied at the boundaries of the outer domain. The boundary values are specified by the National Centers for Environmental Prediction (NCEP) GFS reanalysis data, while the relaxation zone includes 4 grid points inward from the lateral boundary. For the inner (nested) domain, a horizontal grid resolution of 8 km is used, which includes 679 x 283 grid intervals. The vertical grids are stretched as that in the outer domain. The outer (24 km grid spacing) domain is integrated from 8/10/00Z to 8/24/00Z 2006 and initialized by the NCEP GFS reanalysis data, while the inner domain is integrated from 8/11/12Z to 8/18/00Z for the control case (CNTL). These two nested domains are designed to capture the entire lifecycle over Africa for the larger domain and to focus on the development of the pre-Debby MCS/cloud clusters and AEW and their merging for the inner domain.

The following model physics parameterization or representation schemes are chosen for the present simulations:

- Kain-Fritsch cumulus parameterization scheme
- Thompson microphysics parameterization scheme
- YSU PBL parameterization scheme
- Monin-Obukov surface layer scheme
- Unified Noah land-surface processes scheme
- Second-order diffusion term on coordinate surfaces for turbulence and mixing processes
- Horizontal Smagorinsky first-order closure for eddy coefficient option.
- RRTM longwave radiation parameterization scheme
- Dudhia shortwave radiation parameterization scheme

Details of the above schemes and their relevant references can be found in the ARW user manual (Skamarock et al. 2008).

In making the ARW simulations, we found that the numerically simulated results are sensitive to the microphysics parameterization schemes. In order to choose a better scheme, we performed three testing cases with the Thompson, Purdue-Lin, and WSM6 microphysics parameterization schemes (MPSs) which produce slightly different results (Fig. 6). In general, the simulated OLR, relative vorticity and flow fields compared reasonably well with corresponding observed fields except the propagation speeds of the simulated MCCs and MCSs. The Thompson MPS simulates a

propagation speed 7.6 ms^{-1} (Fig. 6a) which compares more favorably with the observed propagation speed of 7.4 ms^{-1} than the 6.4 ms^{-1} simulated by the Purdue-Lin and WSM6 MPSs (Figs. 6b and 6c). Thus, we choose the case with Thompson MPS as the control case (Case CNTL) and the Thompson MPS will be used for the numerical experiments in the rest of the paper.

Figure 7 shows the local minima of the OLR, relative vorticity, and vector wind fields simulated by Case CNTL. Note that the local OLR minima, as denoted by the concentrated red and blue areas in the horizontal belt centered on 10°N , are used as a proxy of MCS or cloud clusters. They compare reasonably well with the locations of the cloud clusters prior to the pre-Debby MCS before 8/16/18Z and the pre-Debby MCS after 8/16/18Z (Fig. 1). In addition, the ARW model simulated wind fields (Fig. 7) are similar to those analyzed by Meteosat-8 (Fig. 1) and NCEP GFS analysis data (Fig. 4). In general, the ARW model is able to capture major features of the pre-Debby MCS/cloud clusters and AEW from observations.

4. ORIGINS OF PRE-DEBBY MCS AND AEW AND THEIR PRECURSORS

4.1 Origins of Pre-Debby MCS and Its Precursors

Figure 8 shows the ARW model simulated outgoing longwave radiation (OLR) fields for the period 8/11/06Z to 8/16/18Z, which can be compared to the pre-Debby MCS and cloud clusters as revealed in the Meteosat-8 infrared for satellite images (Figs. 1a and 1b). The cloud clusters over northern EH, Red Sea, and AS (EH-AS region) (Fig. 1a) are captured by the model at 8/11/06Z (upper right panel of Fig. 8). The simulated convective cloud clusters went through growth, splitting, weakening, and merging processes similar to those shown in the satellite imagery. There are some slight differences in intensity, propagation speed, and timing of convective activities, which are mainly resulted from the lack of model resolution and parameterizations of physical processes, but the agreement is reasonably well in general.

Several series of cloud clusters over the African continent in the $5\text{-}15^\circ\text{N}$ belt can be traced from the area surrounding EH-AS region. In the following discussions, however, we will focus on the convective cloud clusters which lead to the pre-Debby MCS as identified at 8/16/18Z (Fig. 1b). Note that the simulated cloud cluster over the EH-AS region at 8/11/06Z grew rapidly to become three cloud clusters covering a much larger area at 8/11/18Z (Fig. 8). At 8/12/06Z, the two cloud clusters upstream (on the right side) merged into a cloud cluster while the downstream (left) cloud cluster started to propagate downstream and split from the merged upstream cloud cluster over EH. Six hours later (8/12/18Z), both upstream and downstream cloud clusters continued to grow. The downstream cloud cluster has propagated to be over the DF, split completely from the upstream cloud cluster, and continued to propagate downstream at later times. Note that this downstream cloud cluster (located around

(23°E, 10°N)), which was unrelated to the pre-Debby MCS (dashed red arrowed line in the lower right panel of Fig. 8), appeared to have been enhanced by the stationary, diurnally forced cloud cluster over the DF.

The upstream cloud cluster over the EH went through two diurnal cycles until 8/14/18Z. A similar growing and splitting processes occurred again to produce a cloud cluster, which propagated to the lee side of the DF region at 8/15/18Z. This cloud cluster was enhanced by the diurnally forced stationary cloud cluster over the DF and the propagated farther downstream and became the pre-Debby MCS at 8/16/18Z (lower left panel of Fig. 8). During the period 8/14/06Z to 8/16/18Z, the model-simulated major features are consistent with those revealed in the satellite imagery (Figs. 1b and 3). Similar to the period 8/11/06Z to 8/13/18Z (Fig. 8), in addition to the diurnal convective cloud clusters developed over the EH and DF, another convective cloud cluster was advected and split from that over the EH region toward the DF region. The pre-Debby MCS continued to propagate downstream and grew quickly around (10°E, 10°N) when it crossed over the Jos Plateau at 8/17/18Z (Fig. 7). During this period (8/16/18Z to 8/17/06Z), the simulated MCS or cloud cluster is weaker than that revealed in the satellite imagery. Consistent with the satellite imagery, the pre-Debby MCS continued to grow while propagating downstream from 8/17/06Z to 8/22/18Z and eventually triggered the development of Tropical Storm Debby (2006) (Fig. 7).

The continuity nature of convective activities of the cloud clusters prior to the pre-Debby MCS can also be seen from the Hovmoller diagram of OLR field (Fig. 9). The diurnal convection over EH and DF can be seen clearly from this Hovmoller diagram. The advection, splitting, and merging processes among the convective cloud clusters mentioned above can be seen clearly from the figure. The OLR field simulated by the CNTL case is also consistent with the cloud water mixing ratio field, which is equivalent to the OLR field, as shown in Fig. 12a (to be discussed later).

Briefly speaking, the cloud cluster split over EH around 8/11/00Z (Fig. 9) propagated to the DF region and interacted with the diurnal cloud cluster over DF. It took a couple of diurnal cycles to grow and split again from the DF cloud cluster to evolve into the pre-Debby MCS. The splitting processes can be detected in more detail from the 8-km resolution simulations (not shown), but consistent with that of 24-km resolution results (Fig. 9).

4.2 Origins of the Pre-Debby AEW and Its Precursors

The pre-Debby (2006) African easterly wave (AEW) and its precursor are identified by localized cyclonic relative vorticity maximum by using the ARW simulated relative vorticity fields (Figs. 9 and 10). The model-simulated AEW and its precursor can be traced clearly and are collocated with the observed and ARW-simulated pre-Debby MCS or cloud clusters (Figs. 1, 3,

and 7-9). It also indicates that the AEW can be traced back to 35°E, approximately over the EH.

The simulated AEW or vorticity perturbation field of the CNTL case (Fig. 10) is also consistent with the GFS analysis data as shown in Fig. 11 in which we are able to trace the AEW or positive vorticity perturbations back to about 35°E over the western EH at 8/12/06Z more firmly and to southern Arabian Peninsula around 48°E less firmly. In order to examine the possible origin of the pre-Debby AEW located farther to the east of the EH and AS region, we plotted a Hovmoller diagram of the relative vorticity averaged over 10-20°N and 700-500mb from GFS analysis data for the period of 8/2/00Z to 8/16/00Z (Fig. 12b). The approximate track of the local positive vorticity maximum can be traced back to southern Arabian Peninsula and Arabian Sea (~48°E). Note that the Hovmoller diagram of cloud water mixing ratio from satellite imagery (Fig. 3), GFS data (Figs. 4 and 12a) and CNTL case (Figs. 6a, 7, and 8) also shows that the pre-Debby (2006) MCS or convective cloud clusters were also originated from southern Arabian Peninsula near 43°E.

In order to explore this, we performed a case (Case EAST), similar to case CNTL but with the domain shifted eastward from 0° to 100°E (Fig. 2) and the integration time from 8/1/00Z to 8/16/00Z. Figure 13 shows the Hovmoller diagrams of OLR and relative vorticity fields of case EAST. The OLR plot of Fig. 13a corresponds roughly to the cloud water mixing ratio plot of Fig. 12a, which indicate that the convective cloud clusters preceding the pre-Debby MCS was originated around 43°E (Figs. 11 and 12a), while the cyclonic (positive) vorticity perturbation or the precursor of the pre-Debby AEW was originated slightly to the east around 50°E (Fig. 13b) at approximately 8/10/18Z. Although their origins are slightly different, basically they were formed around the same region, i.e. the Sarawat Mountains in southwest Arabian Peninsula, as can be seen from the OLR (Fig. 14) and relative vorticity (Fig. 15) at 8/10/18Z. Figure 14 shows the evolution of ARW model simulated OLR field with time for case EAST. The convective cloud cluster preceding the pre-Debby MCS can be traced back to the southwest Arabian Peninsula near 43°E around 8/10/18Z. Before this time, there were no noticeable signatures of convective cloud cluster (e.g., see the panel of 8/10/06Z in Fig. 14). In fact, this convective cloud cluster was part of the ITCZ which normally exists in August along the southern Arabian Peninsula (Fig. 5). This cloud cluster was moving downstream with the northeasterly wind to EH (~40°E) at later time around 8/11/18Z. At this time, the cloud cluster preceding the pre-Debby MCS is strengthened by the orographically induced diurnal convective cloud cluster over EH. The cloud cluster kept moving westward until around 8/16/18Z when it can be clearly identified as pre-Debby (2006) MCS compared to earlier figures of Case CNTL. Note that the result is consistent with that of case CNTL (Fig. 6a) and also with that of GFS analysis data (not shown). Thus, the convective cloud clusters preceding the pre-Debby MCS were originated from the southwest Arabian Peninsula near

ITCZ around 8/10/18Z. Figure 15 shows the evolution of ARW model simulated relative vorticity field with time for case EAST. The cyclonic vorticity perturbation preceding the pre-Debby AEW can also be traced back to the same location and time, i.e. southwestern Arabian Peninsula near the ITCZ around 8/10/18Z.

In summary, both the convective cloud cluster and cyclonic vorticity perturbation preceding the pre-Debby AEW-MCS system were originated from southwestern Arabian Peninsula in the vicinity of the ITCZ around 8/10/18Z.

4.3 Sources of Cyclonic Vorticity and Convective Cloud Clusters Preceding the Pre-Debby AEW-MCS System

The low-level wind fields at 700mb (Fig. 14) and at 900mb (Fig. 15) suggest that the convective cloud clusters and the cyclonic vorticity perturbations were produced by the cyclonic convergence of the northeasterly wind burst toward the southwestern Arabian Peninsula and the Somali jet, as part of the southwesterly monsoon current associated with the Indian Ocean High, right before 8/10/18Z. Note that the Somali jet is stronger in the lower layer such as 900mb, while the northeasterly wind burst is stronger at the 700 mb than at 900 mb. The northeasterly wind appears to be related to the outbreak of summer "Shamal". A Shamal is a northwesterly or northerly wind blowing over Iraq, Iran, and Saudi Arabia toward Arabian Sea, which is associated with a low over Iran and a high over eastern Mediterranean (e.g., Rao et al. 2003). The strengthening of the Iranian low and the Mediterranean high, and the southeastward extension of the pressure ridge from the high tend to generate the outbreak of summer Shamal. Occasionally, Shamal blows southwestward and interacts with the southwesterly Somali jet to produce a positive vorticity ($\zeta > 0$), which in turn increases the rate of change of relative vorticity ($\partial\zeta/\partial t > 0$) through the convergence term of the vorticity equation, $-(\zeta + \bar{\eta})(\partial\bar{u}/\partial x + \partial\bar{v}/\partial y)$. The cyclonic convergence zone is situated along the coast of Arabian Sea in the vicinity of the ITCZ, coincided approximately with the general location of ITCZ in August (Fig. 5).

The cyclonic (positive) vorticity perturbations, as shown in the north-south Hovmoller diagram averaged over 40-50°E and 700mb-500mb (Fig. 16c), were associated with the northeasterly wind burst and Somali jet as can be seen in the north-south Hovmoller diagram of the U wind (Fig. 16a) and the east-west Hovmoller diagram of the V component of the wind (Fig. 16f). Figures 16a and 16f also indicate that in this area the generation of cyclonic vorticity is dominated by the U component of the wind ($-\partial u/\partial y$) (Fig. 16a) than the V component of the wind ($\partial v/\partial x$) (Fig. 16f). An interesting and important feature of the U component of the wind in this region (40-50°E) is the southward advection of the cyclonic (positive) vorticity perturbations in three time periods started around August 3, 7, and 11 (Figs. 16a, 16b, and 16c). Apparently, these cyclonic vorticity perturbations were generated by the interaction

between the northeasterly wind bursts and the Somali jet (Figs. 16b, 16e, and 16f).

The cyclonic vorticity was generated approximately every 4 days, which might dictate the time interval between AEWs downstream (to the west) over central and western North Africa (Fig. 9). The third cyclonic vorticity perturbation started around 8/11/06Z near southwest Arabian Peninsula eventually evolved into the pre-Debby AEW downstream of northern EH (~38-40°E) as denoted by the long arrow in Fig. 10. Unlike the pre-Debby MCS which can only be identified clearly from satellite imagery starting at 8/16/18Z, the pre-Debby AEW can be traced almost continuously back to 8/11/06Z (Figs. 9, 10, 11, and 15). Thus, the cyclonic vorticity perturbation generated around 8/11/06Z may be identified as the pre-Debby AEW.

The formation of convective cloud clusters in southern Arabian Peninsula during this period (Aug. 2 – 16) (Fig. 16d) occurred around the same times as those of the cyclonic vorticity perturbations (Fig. 16c), i.e. August 3, 7, and 11. This implies that the formation of convective cloud clusters is related to that of cyclonic vorticity perturbations which were driven by the interaction between the northeasterly wind burst and Somali jet, as shown in the north-south Hovmoller diagrams of the 40-50°E averaged U and V wind components (Figs. 16a and 16b). As noted earlier, the convective cloud clusters were generated by the convective heating associated with ITCZ, while the cyclonic vorticity was generated by the cyclonic convergence as shown in the U component of the horizontal wind (Fig. 16a).

In order to explore the synoptic scale environment conducive to the formation of the cyclonic vorticity perturbations and convective cloud clusters preceding the pre-Debby AEW-MCS system, we plotted event and non-event composite fields for cyclonic vorticity perturbations and convective cloud clusters in the vicinity of the southwest Arabian Peninsula (Fig. 17). Based on the OLR, positive relative vorticity, and 700 mb vector wind fields of case EAST, similar to the plots of Figs. 14 and 15, the following event dates are selected: 8/2/18Z, 8/5/18Z, 8/7/18Z, and 8/11/18Z, while the non-event dates selected are: 8/4/06Z, 8/8/06Z, 8/9/06Z, and 8/10/06Z. During the event, the Indian Ocean high was strong and its associated Somali jet penetrated farther to the north along the coast of Arabian sea, and interacted with the northeasterly Shamal to produce strong convergence and cyclonic vorticity there.

5. CONCLUDING REMARKS

In this study, the origins of the mesoscale convective system (MCS)/convective cloud clusters and the African easterly wave (AEW)/vorticity perturbations, which triggered Tropical Storm Debby (2006), were traced back to eastern Africa and southern Arabian Peninsula using satellite imagery, GFS analysis data, and ARW model simulated results.

Based on the analysis of the Meteosat-8 infrared

imagery and GRISAT data, the pre-Debby (2006) MCS was clearly traced back to 8/16/18Z near (20°E, 10°N), which was formed by a series of successive, more or less organized cloud clusters during the period 8/11/00Z to 8/16/18Z. These cloud clusters developed over the area of southwest Arabian Peninsula, Asir Mountains, and Ethiopian Highlands. During this period, the convective cloud clusters went through growing, splitting, advection, weakening, and merging processes, then propagated westward across the North African continent at later times. During these processes, not every individual cloud cluster survived. In fact, some of them propagated faster than the average speed and dissipated while a new MCS or cloud cluster formed. Some of the propagating MCS/cloud clusters and AEW/vorticity perturbations were weakened or split by orographic blocking, but were strengthened or weakened by the diurnal heating or cooling over the mountains. This may help explain the discontinuity of the pre-Debby MCS/convective cloud clusters.

The propagation of the pre-Debby MCS from 8/16/18Z to the Atlantic Ocean was smooth until it encountered the Guinea (Futa Jallon) Highlands (GH). During its passage over GH, the convection developed quicker on the lee and southern sides of the mountains during the period 8/20/00Z to 8/20/06Z. At 8/20/06Z, the pre-Debby MCS split into two cloud clusters, as revealed by the GRISAT data. The downstream cloud cluster continued to propagate westward, while the upstream cloud cluster regrouped and developed into a stronger MCS which then triggered the Tropical Storm Debby (2006) over the ocean after 8/21/00Z. The propagation speed of the pre-Debby MCS during the period 8/16/18Z to 8/21/18Z was slightly faster than the lower end of the climatological mean speed.

Using the GFS data, the pre-Debby cloud clusters was traced back to about 42°E, over EH-AS region and Arabian Peninsula. Three to four convective systems or cloud clusters co-existed along the belt of 5-15°N, which were associated with the ITCZ. The ARW simulation (case CNTL) was able to capture the pre-Debby MCS/cloud clusters as observed in the satellite imagery and GFS analysis data for the period 8/11/00Z to 8/16/18Z except discrepancies existed in their intensity, timing of occurrence and dissipation, and faster propagation speed. The simulated pre-Debby cloud clusters went through growth, splitting, weakening, and merging processes, and were traced to the area surrounding EH-AS region. The simulated diurnal convection over EH and DF can be seen clearly from this Hovmoller diagram. The pre-Debby cloud cluster split from the diurnal cloud cluster over EH around 8/11/00Z propagated to the DF region and interacted with the diurnal cloud cluster over DF. It took a couple of diurnal cycles to grow and split again from the DF cloud cluster to evolve into the pre-Debby MCS.

The ARW-simulated relative vorticity fields indicated that the pre-Debby AEW or cyclonic vorticity perturbation was originated around 50°E, slightly to the east of the origin of the pre-Debby cloud clusters, at 8/10/18Z. Basically, the pre-Debby AEW and cloud clusters were formed around 8/10/18Z in southwest

Arabian Peninsula in the vicinity of the ITCZ near the Sarawat Mountains. The cloud clusters were moving downstream with the northeasterly wind to EH (~40°E) around 8/11/18Z, and strengthened by the orographically induced diurnal convective cloud cluster there. These cloud clusters kept moving westward until around 8/16/18Z when it can be clearly identified as pre-Debby (2006) MCS compared to earlier figures.

It was found that the convective cloud clusters and the cyclonic vorticity perturbations were produced by the cyclonic convergence of the northeasterly wind burst toward the southwestern Arabian Peninsula and the Somali jet right before 8/10/18Z. The northeasterly wind might be related to the outbreak of “*Shamal*” wind, which was associated with the strengthening of the Iranian low and the southeastward extension of the pressure ridge from the Mediterranean high. The northeasterly Shamal appeared to interact with the southwesterly Somali jet to produce a cyclonic vorticity ($\zeta > 0$), which in turn increased the rate of change of relative vorticity ($\partial\zeta/\partial t > 0$) through the convergence term of the vorticity equation ($-(\zeta + f)\partial u/\partial x + \partial v/\partial y$). The cyclonic convergence zone is situated along the coast of Arabian Sea in the vicinity of the ITCZ. The argument was supported by the analyses of east-west Hovmoller diagrams of U and V components of the wind, and relative vorticity and cloud water mixing ratio, and north-south Hovmoller diagrams of U and V components of the wind. In addition, it was found that the cyclonic vorticity was generated approximately every 4 days, which might dictate the time interval between AEWs downstream (to the west) over central and western North Africa. The cyclonic vorticity perturbation started around 8/11/06Z near southwest Arabian Peninsula eventually evolved into the pre-Debby AEW downstream of northern EH (~38-40°E). Unlike the pre-Debby MCS which can only be identified clearly from satellite imagery starting at 8/16/18Z, the pre-Debby AEW can be traced almost continuously back to 8/11/06Z.

In summary, the pre-Debby (2006) MCS can be clearly traced back to 8/16/18Z while the convective cloud clusters preceding the MCS can be traced to southwest Arabian Peninsula. The AEW/vorticity perturbations can be traced more continuously to the southwest Arabian Peninsula. Thus, we may conclude that the pre-Debby (2006) MCS-AEW system was originated from the southwest Arabian Peninsula in the vicinity of the ITCZ. The sources of the convective cloud clusters and vorticity perturbations were attributed to the cyclonic convergence of northeasterly Shamal wind and the Somali jet, especially when the Mediterranean High shifted toward east with high pressure ridge extended farther to the southeast and the Indian Ocean high strengthened and its associated Somali jet penetrated farther to the north. The cyclonic vorticity perturbations were strengthened by the vorticity stretching associated with convective cloud clusters and the convective cloud clusters are strengthened by the diurnal convection over the Sarawat Mountains, Asir Mountains, Ethiopian Highlands, and Darfur Mountains downstream of the genesis region – southwest Arabian Peninsula. The

situation may be summarized in the conceptual model shown in Fig. 18.

In general, the ARW simulated pre-Debby AEW/vorticity perturbations and MCS/convective cloud clusters were in good agreement with satellite imagery and global (GFS) model results. However, some discrepancies still existed in their intensity, timing of occurrence and dissipation, and propagation speed. This might be contributed by several factors, such as the relatively coarse resolution of the model, initialization from the global analysis data (GFS), and sensitivity to parameterization schemes. For example, in making the simulations, the ARW model was sensitive to parameterization schemes of physical processes, such as the Thompson, Purdue-Lin, and WSM6 microphysics parameterization as demonstrated in Fig. 7. Similar phenomenon might happen in other types of parameterization, such as cumulus parameterization and planetary parameterization. Thus, more sensitivity tests are needed to make an optimal combination of parameterizations.

In this study, we have focused on tracing the origins of the pre-Debby MCS/convective cloud clusters and pre-Debby AEW/vorticity perturbations without paying enough attention to the formation of generation mechanisms of these systems. A further study is required to understand exact mechanisms. Such a study might involve a more thorough analysis of global data, and perform a systematic sensitivity tests on isolating forcing mechanisms, such as deactivate sensible and/or latent heating, and removing mountains. In order to generalize the finding of the origins and the formation mechanism(s) of a pre-TC MCS/cloud clusters and AEW/vorticity perturbations, we have to investigate more cases by performing climatological studies and synoptic in the vicinity of their genesis region.

ACKNOWLEDGMENTS: The authors would like to thank Dr. Solomon Billign, the Director of NOAA ISET Center, for his continuous encouragement in pursuing this study. This research was supported by the National Oceanic and Atmospheric Administration Educational Partnership Program under Cooperative Agreement No: NA06OAR4810187.

6. REFERENCES

- AMMA 2006: African Monsoon Multidisciplinary Analysis: <http://amma-international.org/>.
- Berry, G. J., and C. Thorncroft, 2005: Case study of an intense African easterly wave. *Mon. Wea. Rev.*, **133**, 752-766.
- Bister, M., and K. A. Emanuel, 1997: The genesis of Hurricane Guillermo: TEXMEX analysis and a modeling study. *Mon. Wea. Rev.*, **125**, 2662-2682.
- Burpee, R. W., 1972: The origin and structure of easterly waves in the lower troposphere of North Africa. *J. Atmos. Sci.*, **29**, 77-90.
- Burpee, R. W., 1974: Characteristics of the North African easterly waves during the summers of 1968 and 1969. *J. Atmos. Sci.*, **31**, 1556-1570.
- Burpee, R. W., 1974: Characteristics of the North African easterly waves during the summers of 1968 and 1969. *J. Atmos. Sci.*, **31**, 1556-1570.
- Carlson, T. N., 1969: Synoptic histories of three African disturbances that developed into Atlantic hurricanes. *Mon. Wea. Rev.*, **97**, 256-276.
- Chang, C. B., 1993: Impact of desert environment on the genesis of African wave disturbances. *J. Atmos. Sci.*, **50**, 2137-2145.
- Charney, J. G., and M. E. Stern, 1962: On the stability of internal baroclinic jets in a rotating atmosphere. *J. Atmos. Sci.*, **19**, 159-172.
- Chen, S.-H., and W.-Y. Sun, 2002: A one-dimensional time-dependent cloud model, *J. Meteor. Soc. Japan*, **80**, 99-118.
- Chen, T.-C., 2006: Characteristics of African easterly waves depicted by ECMWF reanalysis for 1991-2000. *Mon. Wea. Rev.*, **134**, 3539-3566.
- Cotton W. R., R. L. George, P. J. Wetzell, and R. L. McAnelly, 1983: A long-lived mesoscale convective complex. Part I: The mountain-generated component. *Mon. Wea. Rev.*, **111**, 1893-1918.
- Farfan, L. M., and J. A. Zehnder, 1997: Orographic influence in the synoptic-scale circulation associated with the genesis of Hurricane Guillermo. *Mon. Wea. Rev.*, **125**, 2683-2698.
- Fink, A. H., and A. Reiner, 2003: Spatio-temporal variability of the relation between African easterly waves and West African squall lines in 1998 and 1999. *J. Geophys. Res.*, **108**, 4332, doi:10.1029/2002JD002816.
- Frank, N. L., 1970: Atlantic tropical systems of 1969. *Mon. Wea. Rev.*, **98**, 307-314.
- Glickman, T. S. (ed.), 2000: *Glossary of Meteorology*. 2nd Ed., Amer. Meteor. Soc., 855pp.
- Goldenberg, S. B., and L. J. Shapiro, 1996: Physical mechanisms for the association of El Niño and West African rainfall with Atlantic major hurricane activity. *J. Clim.*, **9**, 1169-1187.
- Grist, J. P., S. E. Nicholson, and A. L. Barcion, 2002: Easterly wave over Africa. Part II: Observed and modeled contrast between wet and dry years. *Mon. Wea. Rev.*, **130**, 212-225.
- Hill, C. M., and Y.-L. Lin, 2003: Initiation of a mesoscale convective complex over the Ethiopian Highlands preceding the genesis of Hurricane Alberto (2000). *Geophys. Res. Lett.*, **30**, No. 5, 1232 doi:10.1029/2002GL016655, 2003.
- Houze, R. A., 1993: *Cloud Dynamics*. Academic Press, 612pp.
- Hsieh, J.-S., and K. H. Cook, 2005: Generation of African easterly wave disturbances: Relationship to the African easterly jet. *Mon. Wea. Rev.*, **133**, 1311-1327.
- Hsieh, J.-S., and K. H. Cook, 2007: A study of the energetics of African easterly waves using a regional climate model. *J. Atmos. Sci.*, **64**, 2212-2230.
- Kwon, H. J., 1989: A re-examination of the genesis of African waves. *J. Atmos. Sci.*, **46**, 3621-3631.
- Laing, A., R. Carbone, V. Levizzani, and J. Tuttle, 2008: The propagation and diurnal cycles of deep

- convection in northern tropical Africa. *Quart. J. Roy. Meteor. Soc.*, **134**, 93-109.
- Laing, A. G., and J. M. Fritsch, 1993: Mesoscale convective complexes in Africa. *Mon. Wea. Rev.*, **121**, 2254-2263.
- Landsea, C. W., 1993: A climatology of intense (or major) Atlantic hurricanes. *Mon. Wea. Rev.*, **121**, 1703-1713.
- Lin, Y.-L., 2007: *Mesoscale Dynamics*. Cambridge University Press, 630pp.
- Lin, Y.-L., K. E. Robertson, and C. M. Hill, 2005: Origin and propagation of a disturbance associated with an African easterly wave as a precursor of Hurricane Alberto (2000). *Mon. Wea. Rev.*, **133**, 3276-3298.
- Mass, C., 1979: A linear primitive equation model of African wave disturbances. *J. Atmos. Sci.*, **36**, 2075-2092.
- Mekonnen, A., C. D. Thorncroft, and A. R. Aiyer, 2006: Analysis of convection and its association with African easterly waves. *J. Climate*, **19**, 5405-5421.
- Mozer, J. B., and J. A. Zehnder, 1995: Lee vorticity production by large-scale tropical mountain ranges. part ii: a mechanism for the production of African waves. *J. Atmos. Sci.*, **53**, 539-549.
- NOAA, 2006: NOAA CPC FEWS - NET Rainfall Estimate (mm): For the Northern Africa Rainfall Climatology, August 2006. (http://www.cpc.ncep.noaa.gov/products/fews/rfe1_s.html)
- Payne, S. W., and M. M. McGarry, 1977: The relationship of satellite inferred convective activity to easterly waves over West Africa and the adjacent ocean during phase III of GATE. *Mon. Wea. Rev.*, **105**, 413-420.
- Pielke, Jr., R. A., and C. W. Landsea, 1998: Normalized hurricane damages in the United States: 1925-95. *Weather Forecasting*, **13**, 621-631.
- Pytharoulis, I., and C. Thorncroft, 1999: The low-level structure of African easterly waves in 1995. *Mon. Wea. Rev.*, **127**, 2266-2280.
- Rao, P. G., H. R. Hatwar, H. H. Al-Sulaiti, and A. H. Al-Mulia, 2003: Summer shamals over the Arabian Gulf. *Weather*, **58**, 472 - 478.
- Reed, R. J., D. C. Norquist, and E. E. Recker, 1977: The structure and properties of African wave disturbances as observed during phase III of GATE. *Mon. Wea. Rev.*, **105**, 317-333.
- Rennick, M. A., 1976: The generation of African waves. *J. Atmos. Sci.*, **33**, 1955-1969.
- Seo, H., M. Jochum, R. Murtugudde, A. J. Miller, and J. O. Roads, 2008: Precipitation from African easterly waves in a coupled model of the tropical Atlantic. *J. Climate*, **21**, 1417-1431.
- Simmons, A. J., 1977: A note on the instability of the African easterly jet. *J. Atmos. Sci.*, **34**, 1670-1674.
- Skamarock, W. C., J. B. Klemp, J. Dudhia, D. O. Gill, D. M. Barker, M. G. Duda, X.-Y. Huang, W. Wang, and J.G. Powers, 2008: A description of the advanced research WRF version 3. NCAR technical note, 113 pp. (also see http://www.mmm.ucar.edu/wrf/users/docs/arw_v3.pdf)
- Thorncroft, C. D., 1995: An idealized study of African easterly waves. *J. Atmos. Sci.*, Part III: More realistic basic states. *Quart. J. Roy. Meteor. Soc.*, **121**, 1589-1614.
- Thorncroft, C. D., and B. J. Hoskins, 1994a: An idealized study of African easterly waves. Part I: A linear view. *Quart. J. Roy. Meteor., Soc.*, **120**, 953-982.
- Thorncroft, C. D., and B. J. Hoskins, 1994b: An idealized study of African easterly waves. Part II: A nonlinear view. *Quart. J. Roy. Meteor., Soc.*, **120**, 983-1015.
- Thorncroft, C. D., N. M. Hall, and G. N. Kiladis, 2008: Three-dimensional structure and dynamics of African easterly waves. Part III: Genesis. *J. Atmos. Sci.*, **65**, 3596-3607.
- Wetzel, P. J., W. R. Cotton, and R. L. McAnelly, 1983: A long-lived mesoscale convective complex. Part II: Evolution and structure of the mature complex. *Mon. Wea. Rev.*, **111**, 1919-1937.

Acronym	Meaning
AEW	African easterly waves
AP	Arabian Peninsula
ARW	Advance Research WRF model
AEW-MCS	Coupled AEW and MCS system
AS	Asir Mountains
AS-EH	Asir Mountains and Ethiopian Highlands region
DF	Darfur Mountains
EH	Ethiopian Highlands
GFS	Global Forecast System
GH	Guinea (Futa Jallon) Highlands
GRISAT	Grid satellite data
ITCZ	Inter-Tropical Convergence Zone
JP	Jos Plateau
MCS	Mesoscale Convective System
MDR	main development region (in Atlantic Ocean)
OLR	outgoing longwave radiation
TC	tropical cyclone
SM	Sarawat Mountains (in southwest Arabian Peninsula)
WRF	Weather Research Forecast model

Table 1: List of acronyms.

Cases	Features
CNTL	Control Experiment: Outer domain: (40°W, 10°S) – (60°E, 40°N); $\Delta x = 24$ km; 8/10/00Z – 8/24/00Z Inner domain: (10°W, 0°) – (50°E, 20°N); $\Delta x = 8$ km; 8/11/12Z – 8/18/00Z (see Fig. 2 for domain coverage.)
EAST	Domain: (0°, 10°S) – (100°E, 40°N); $\Delta x = 24$ km; 8/1/00Z – 8/16/00Z (Similar to CNTL; see Fig. 2 for domain coverage.)

Table 2: List of ARW numerical experiments.

Fig. 1 ([http://mesolab.ncat.edu/publications \(web\)/AMS_preprint Fig 1.pdf](http://mesolab.ncat.edu/publications(web)/AMS_preprint_Fig_1.pdf)) Meteosat-8 infrared (IR) clouds and wind vectors for every 6h starting from 8/11/00Z to 8/22/18Z 2006 (AMMA 2006). The center latitude is 10°N. Track of the approximate locations of the pre-Debby (2006) MCS or convective cloud clusters are highlighted by dotted yellow and white circles. The dotted white circles denote the cloud clusters which were not related to the pre-Debby MCS identified at 8/16/18Z. The right (left) yellow line denotes the diurnal convection mode (diurnal cycle) of orographic cloud clusters over the Ethiopian Highlands (Darfur Mountains). The wind vectors were analyzed by Meteosat-8 and are denoted as: blue for 400-599 mb, yellow for 600-799 mb, and green for 800-950 mb).

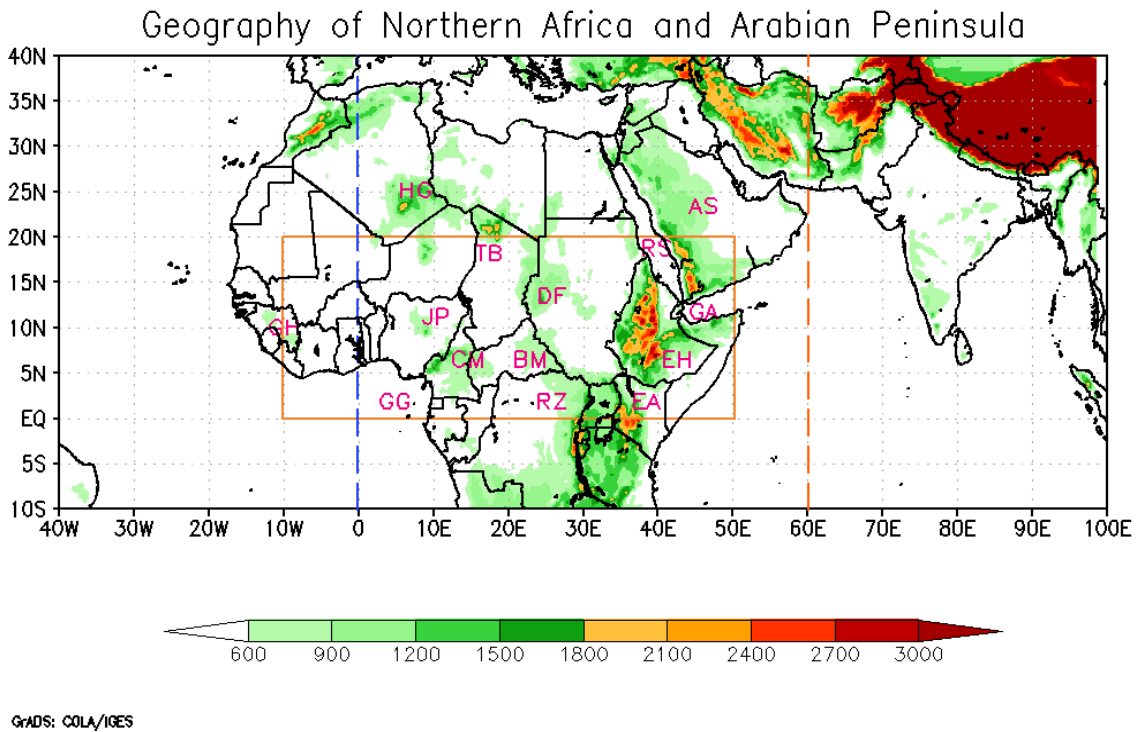


Fig. 2: Geography for Africa (north of 10°S) and southern Arabia Peninsula. Labels indicate major geographic features: AS – Asir Mountains; BM – Bongo Massif; CM – Cameron Highlands; DF – Darfur Mountains; EA – Eastern Arc Mountains; EH – Ethiopian Highlands; GH – Guinea (Futa Jallon) Highlands; GA – Gulf of Aden; GG – Gulf of Guinea; HG – Hoggar Mountains; JP – Jos Plateau; RZ – Ruwenzori Mountains; TB – Tibesti Mountains. The outer domain of the CNTL simulation is (40°W, 10°S) to (60°E, 40°N), while the inner domain of the CNTL case (8-km resolution) is enclosed by the brown lines. The domain of EAST simulation is from (0°, 10°S) to (100°E, 40°N).

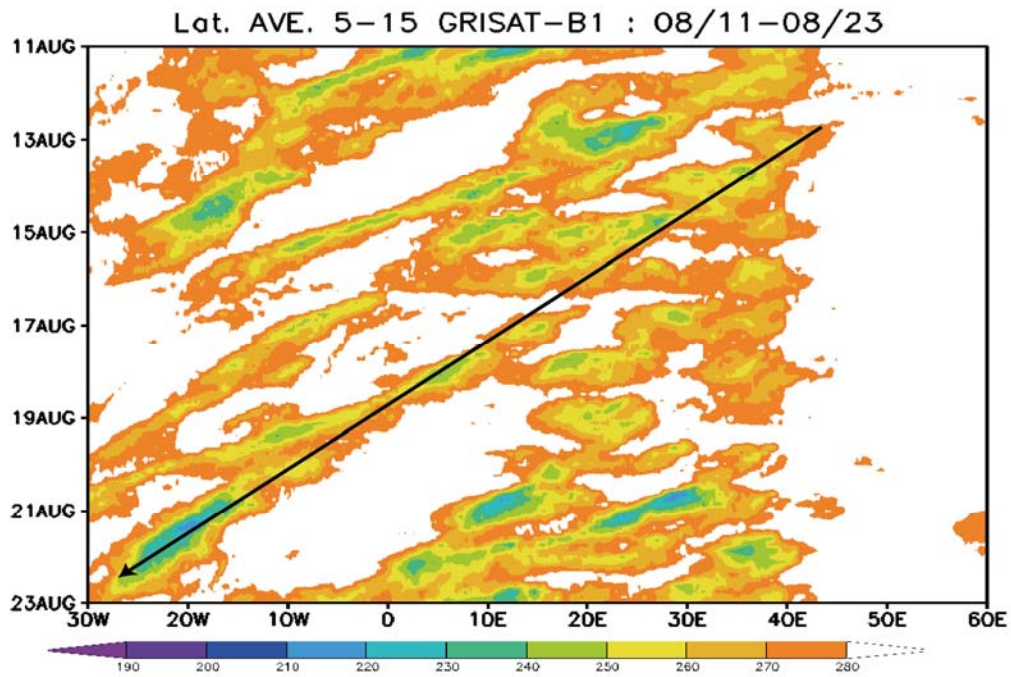


Fig. 3: Hovmoller diagrams of 5-15°N averaged brightness temperature as observed from grid satellite (GRISAT) data. The black straight line denotes the approximate track of the pre-Debby MCS and the convective cloud clusters (CCCs).

Fig. 4 ([http://mesolab.ncat.edu/publications%20\(web\)/AMS_preprint_Fig_4.pdf](http://mesolab.ncat.edu/publications%20(web)/AMS_preprint_Fig_4.pdf)): Atmospheric column cloud water mixing ratio (kg kg^{-1}) from GFS analysis data (8/10/06Z – 8/16/18Z).

NOAA CPC FEWS–NET Rainfall Estimate (mm): for the Africa Rainfall Climatology

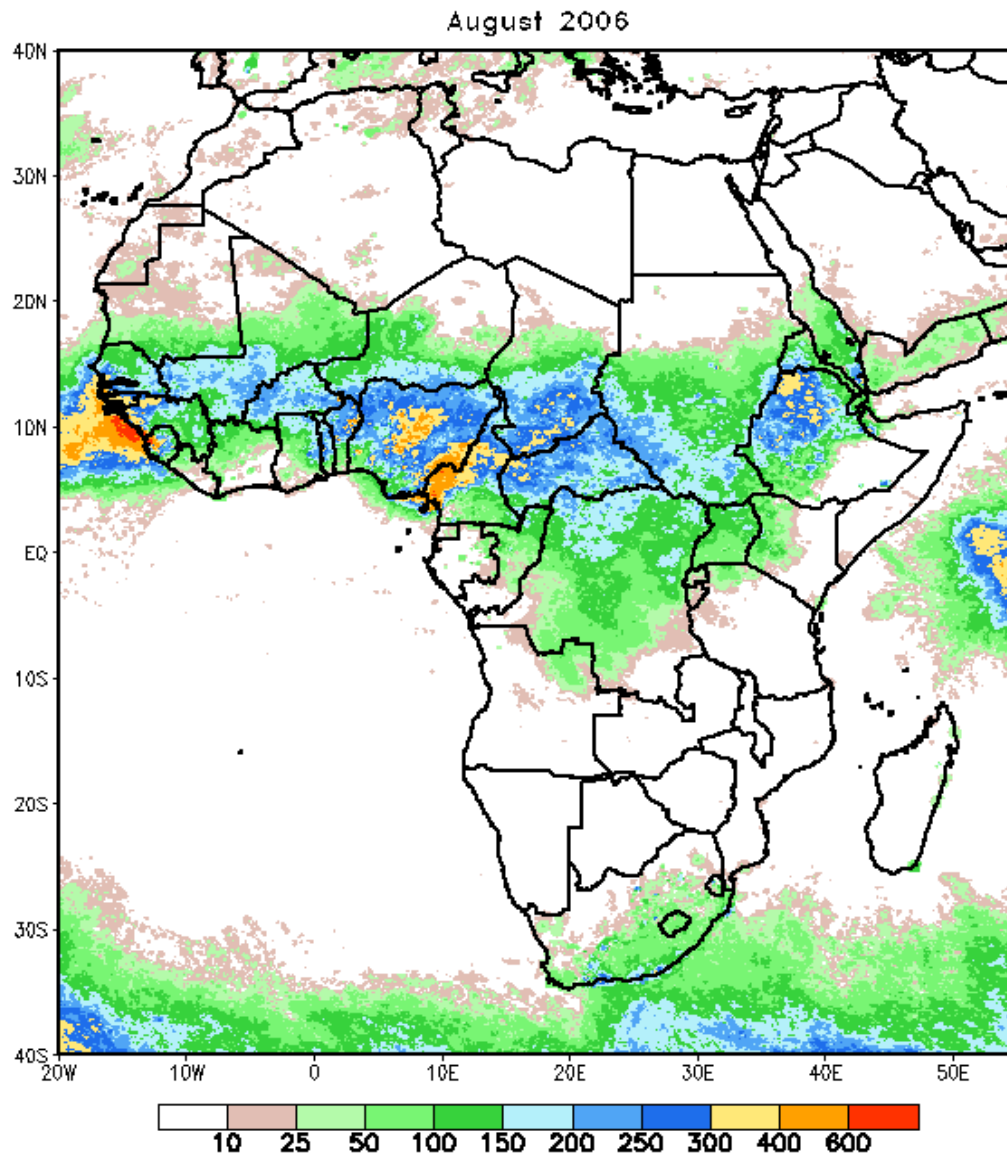


Fig 5: The NOAA Climate Prediction Center (CPC) Famine Early Warning System (FEWS) net rainfall estimate (mm) for the Northern Africa rainfall climatology for the month of August 2006 (NOAA 2006).

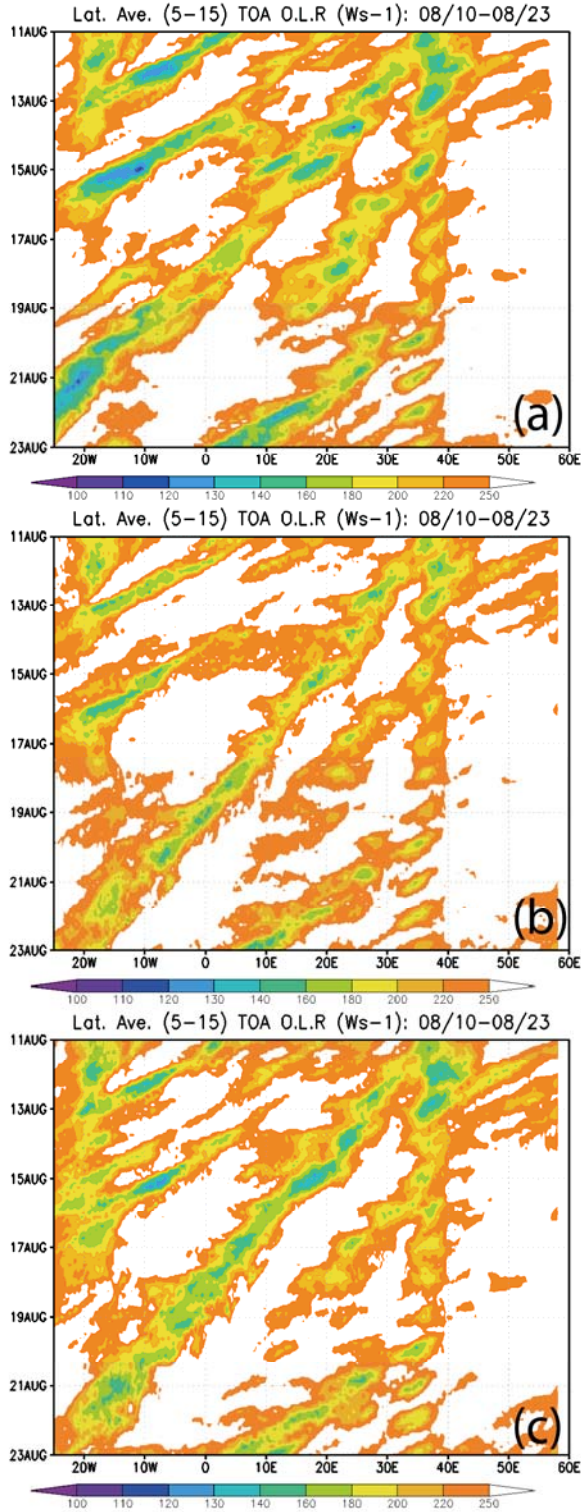


Fig. 6: Hovmoller diagrams of 5-15°N averaged OLR from WRF simulations using (a) Thompson microphysics parameterization scheme (MPS), (b) Purdue-Lin MPS, and (c) WSM6 MPS.

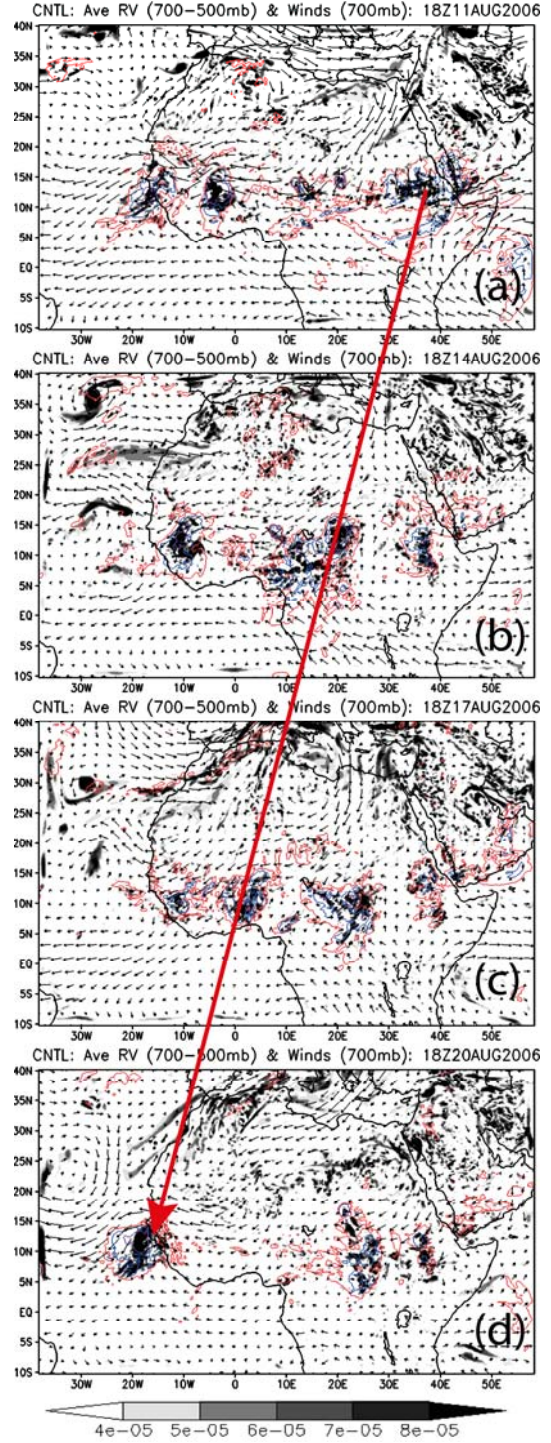


Fig. 7: (Case CNTL): The Outgoing longwave radiation (OLR, color-contoured), 700mb horizontal wind vector, and 500-700mb averaged relative vorticity (gray-shaded; in s^{-1}) fields simulated by the ARW model with 24-km resolution for Case CNTL. Contours for OLR are: red for 220K, blue for 130K, and purple for 95K. The MCS-AEW system is denoted by the red arrow line.

Fig. 8 ([http://mesolab.ncat.edu/publications%20\(web\)/AMS_preprint_Fig_8.pdf](http://mesolab.ncat.edu/publications%20(web)/AMS_preprint_Fig_8.pdf)) (Case CNTL): The outgoing longwave radiation (OLR) fields for every 12h starting from 8/11/00Z to 8/16/18Z 2006 simulated by the 24-km resolution (outer domain) ARW model. The approximate positions of convective cloud clusters preceding the pre-Debby MCS is denoted by long dashed red arrow line.

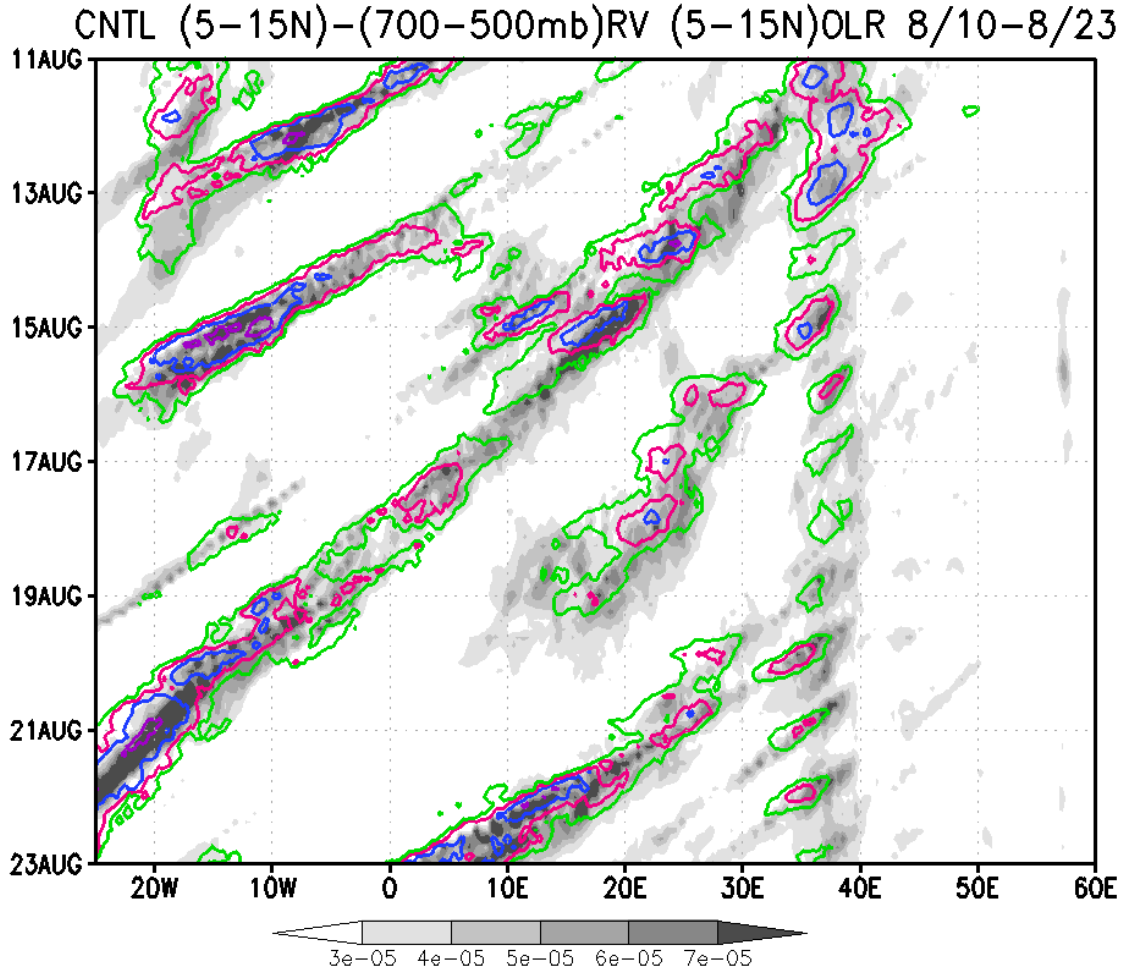


Fig. 9 ([http://mesolab.ncat.edu/publications%20\(web\)/AMS_preprint_Fig_10.pdf](http://mesolab.ncat.edu/publications%20(web)/AMS_preprint_Fig_10.pdf)) (Case CNTL): Hovmoller diagrams for the averaged 5-15°N OLR and averaged 700-500 mb and 5-15°N relative vorticity (s^{-1}) simulated by the 24-km resolution ARW model for case CNTL.

Fig.10 ([http://mesolab.ncat.edu/publications%20\(web\)/AMS_preprint_Fig_10.pdf](http://mesolab.ncat.edu/publications%20(web)/AMS_preprint_Fig_10.pdf)) (Case CNTL): The averaged 500-700mb cyclonic relative vorticity (shaded; in s^{-1}) and vector wind fields based on the 24-km resolution (outer domain) ARW simulated results for every 12h starting from 8/11/06Z to 8/16/18Z. The relative vorticity areas higher than $2.0 \times 10^{-5} s^{-1}$ are shaded. The black lines denote the propagation of the pre-Debby AEW and its precursor (cyclonic vorticity perturbation).

Fig. 11 ([http://mesolab.ncat.edu/publications%20\(web\)/AMS_preprint_Fig_11.pdf](http://mesolab.ncat.edu/publications%20(web)/AMS_preprint_Fig_11.pdf)): The 700-500mb averaged relative vorticity and 700mb wind vectors from GFS analysis data for 8/10/06Z to 8/16/18Z. The red solid (dashed) line denotes the approximate (possible) track of pre-Debby AEW/vorticity perturbation.

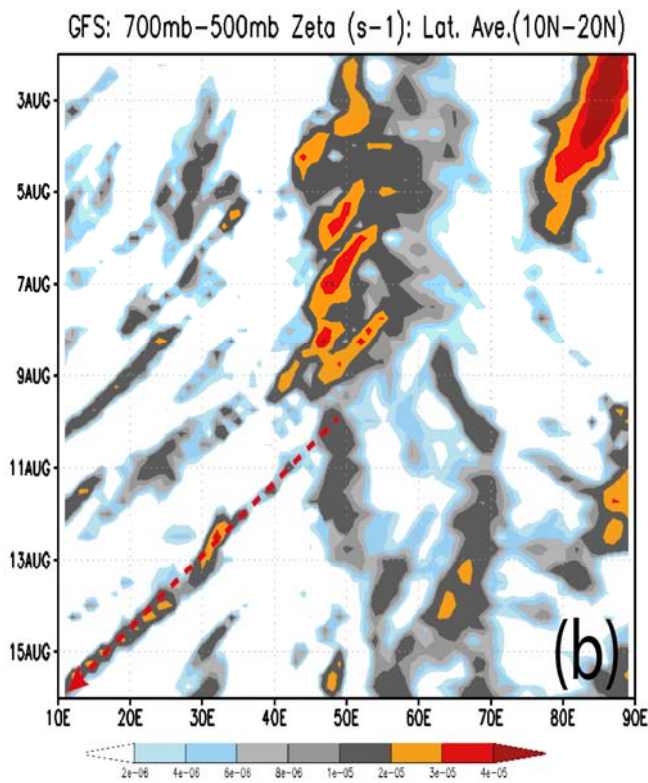
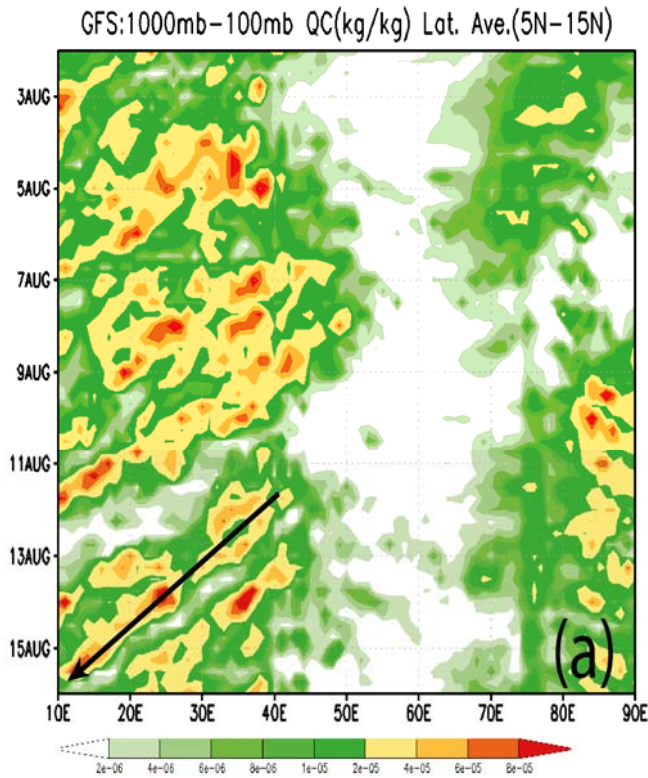


Fig. 12 (GFS): Hovmöller diagrams for: (a) cloud water mixing ratio ($kg\ kg^{-1}$) averaged over 5-15°N and (b) relative vorticity (s^{-1}) averaged over 10-20°N and 700-500 mb from the GFS data.

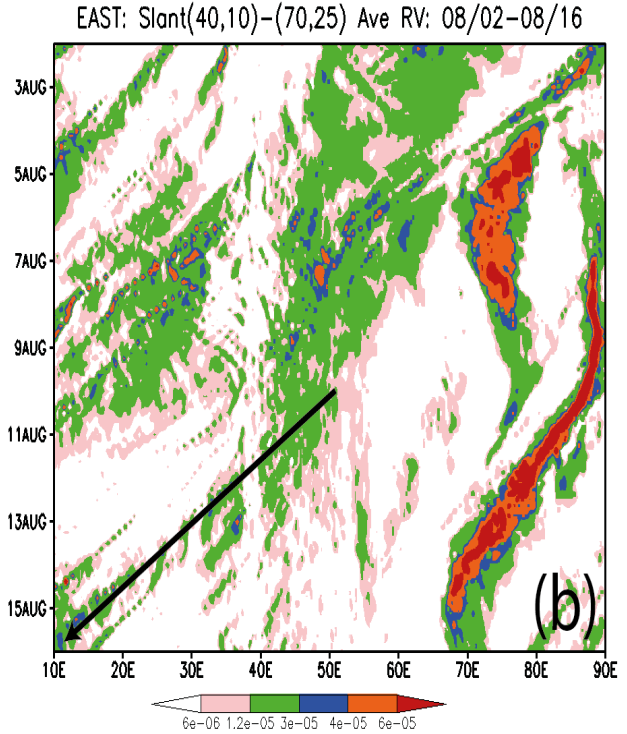
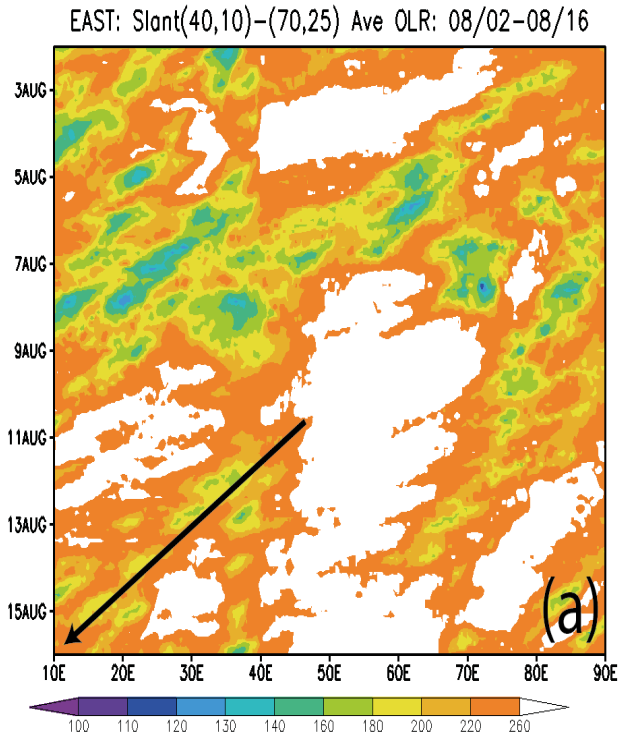
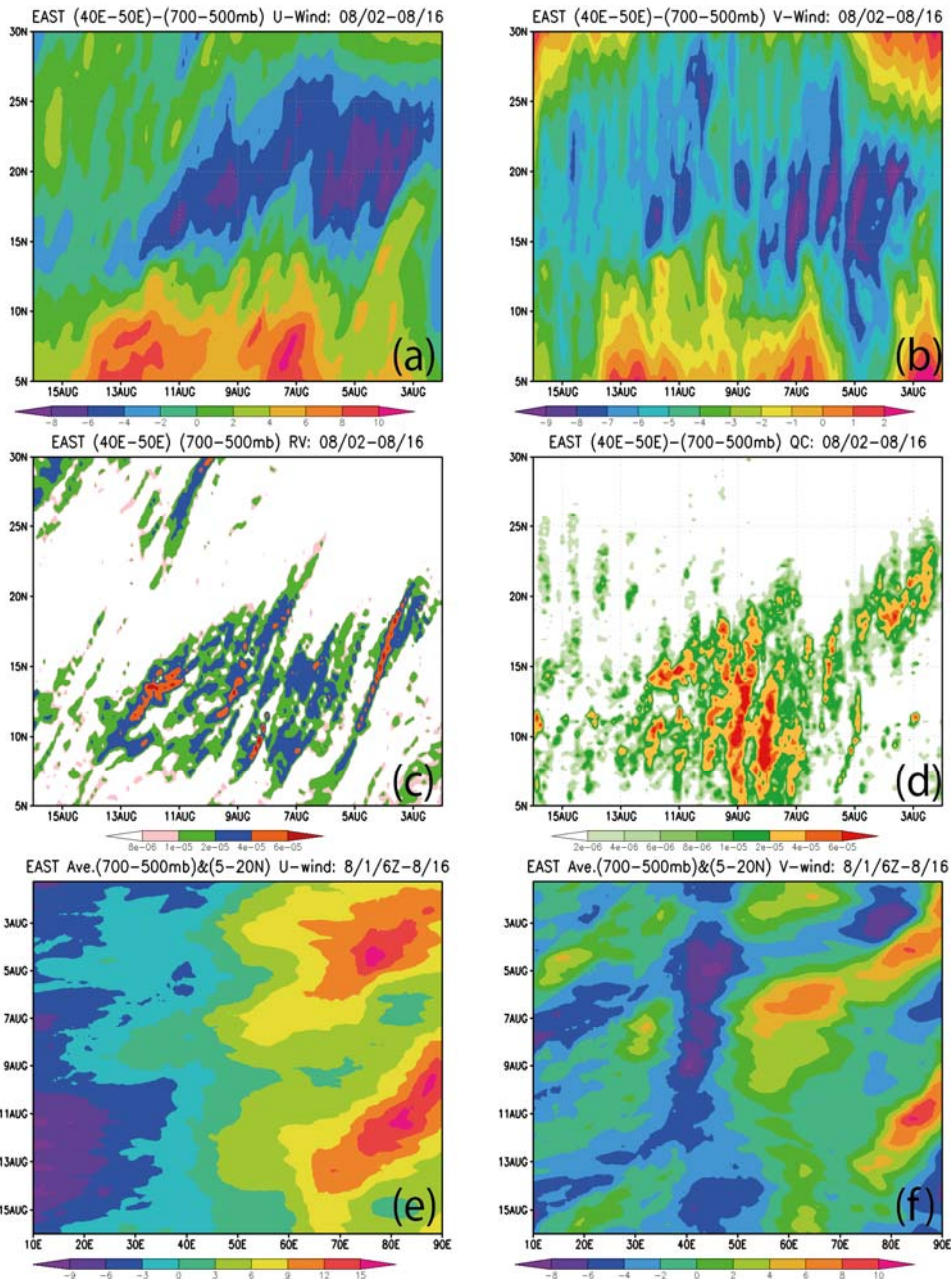


Fig. 13 (Case EAST): Hovmöller diagrams for: (a) OLR and (b) relative vorticity (s^{-1}) averaged over 5-15°N to the west of 40°E, and 20-30°N to the east of 70°E, and over a 10° band along a line from (40°E, 10°N) to (70°E, 25°N) (approximately along the southern Arabian Peninsula), as simulated by the 24-km resolution ARW model for case EAST.

[Fig. 14](#) (Case EAST): The OLR (outgoing longwave radiation) and 700 mb vector wind fields of Case EAST based on the 24-km resolution ARW simulated results for every 12h from 8/8/06Z to 8/13/18Z. The location of the precursor of pre-Debby MCS is denoted by a dashed circle at 8/10/18Z and by a long red arrow line afterwards.

[Fig. 15](#) (Case EAST): The cyclonic relative vorticity averaged over 500-700 mb and the 900 mb vector wind fields of Case EAST based on the 24-km resolution ARW simulated results for every 12h from 8/8/06Z to 8/13/18Z. The location of the precursor of pre-Debby AEW is denoted by a dashed circle at 8/10/18Z and by a long blue arrow line afterwards.



[Fig. 16](#) (EAST): North-South Hovmöller diagrams based on ARW simulated EAST case for 8/2/00Z to 8/16/00Z: (a) U wind (ms^{-1}), (b) V wind (ms^{-1}), (c) cyclonic (positive) relative vorticity (s^{-1}), and (d) cloud water mixing ratio (kg/kg) averaged over 40-50°E and 700-500mb. Panels (c) and (d) are the same as (a) and (b), but for East-West Hovmöller diagrams of 5-20°N and 700-500mb averaged U and V, respectively.

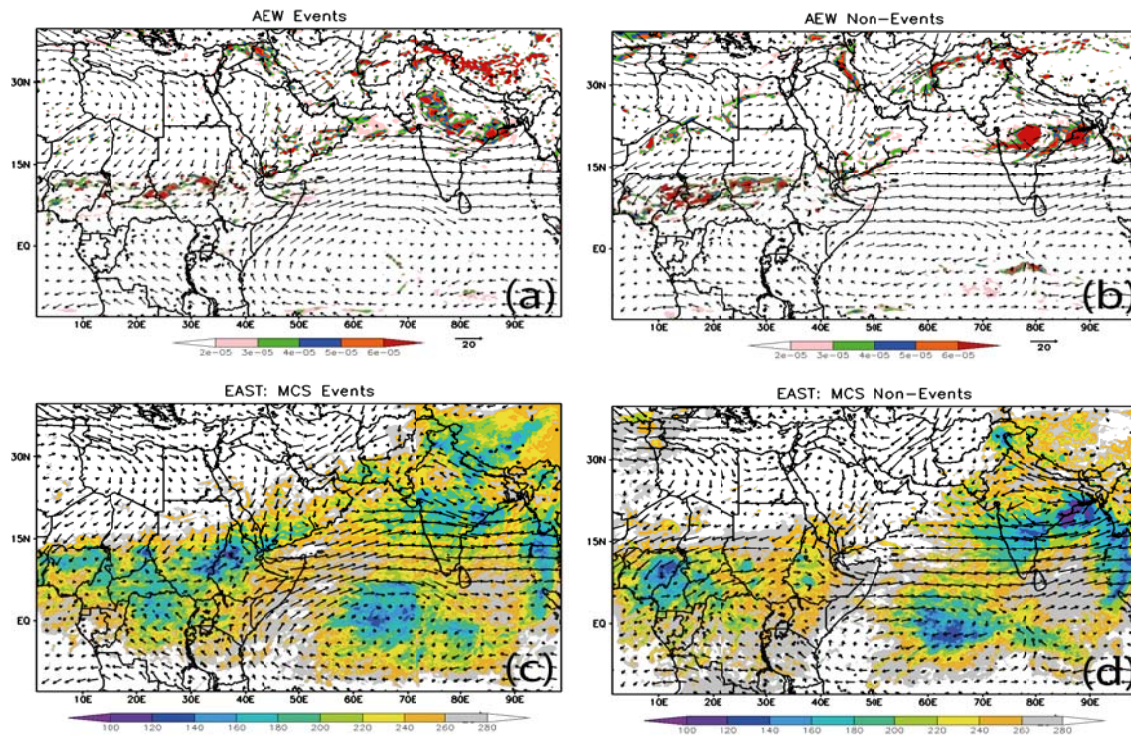


Fig. 17: Composite 700 mb vector wind, 700 – 500 mb average cyclonic (positive) vorticity, and OLR fields for pre-Debby (2006) AEW event (a) and non-event (b), and for pre-Debby (2006) convective cloud clusters event (c) and non-event (d). Event is defined as the occurrence of AEW or convective cloud clusters over southwest Arabian Peninsula.

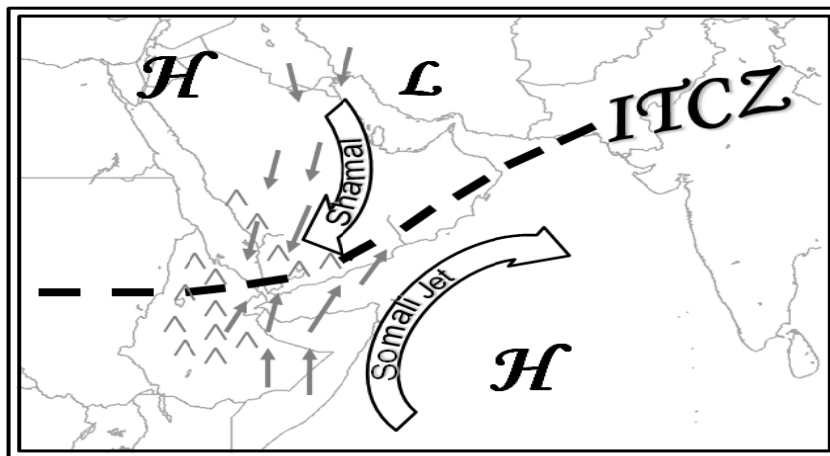


Fig. 18: A conceptual model of the generation of cyclonic vorticity perturbations and convective cloud clusters preceding the pre-Debby (2006) AEW-MCS system. The sources of the convective cloud clusters and vorticity perturbations were attributed to the cyclonic convergence of northeasterly Shamal wind and the Somali jet, especially when the Mediterranean High shifted toward east with high pressure ridge extended farther to the southeast and the Indian Ocean high strengthened and its associated Somali jet penetrated farther to the north. The cyclonic vorticity perturbations were strengthened by the vorticity stretching associated with convective cloud clusters and the convective cloud clusters are strengthened by the diurnal convection over the Sarawat Mountains, Asir Mountains, Ethiopian Highlands, and Darfur Mountains downstream of the genesis region – southwest Arabian Peninsula.